ACS Sustainable Chemistry & Engineering

Research Article

Cite This: ACS Sustainable Chem. Eng. 2018, 6, 7468−7474

pubs.acs.org/journal/ascecg

Thermoelectric Properties of Thermally Reduced Graphene Oxide Observed by Tuning the Energy States

Hyunwoo Bark,[†] Museok Ko,[†] Mijung Lee,[†] Wonmok Lee,[‡] Byunghee Hong,[§] and Hyunjung Lee*[,†]

[†]School of Advanced Material Engineering, Kookmin University, Jeongneung-ro 77, Seongbuk-gu, Seoul, 02707, Republic of Korea

[‡]Department of Chemistry, Sejong University, Neungdong-ro 209, Gwangjin-gu, Seoul, 05006, Republic of Korea

[§]Department of Chemistry, Seoul National University, Gwanak-ro 1, Gwanak-gu, Seoul, 08826, Republic of Korea

Supporting Information

ABSTRACT: Reduced graphene oxide (rGO) possesses a similar electronic structure to graphene but can be synthesized on a larger scale. Hence, rGO is considered as an attractive alternative to graphene. Here we report the carrier transport properties of thermally reduced graphene oxide (TrGO) as a function of reduction temperature. The transfer curve of a field effect transistor fabricated with TrGO exhibited ambipolar properties, and the charge neutrality point of TrGO was shifted from negative to positive as the reduction temperature increased. Furthermore, as revealed in Arrhenius plots of the carrier densities and carrier mobilities, TrGO behaved as a metallic conductor at all reduction temperatures. To investigate the effect of reduction temperature on the thermoelectric properties of TrGO, the Seebeck coefficients of the fabricated TrGOs were calculated from the transfer curve using Mott's equation for metallic materials. All samples showed ambipolar carrier transport. At V_g = 0 V, the Seebeck coefficient switched sign from negative to positive as the reduction temperature became higher, indicating that electron and hole carrier transport dominates at higher and lower reduction temperature, respectively. The calculated Seebeck coefficients at zero gate bias were compared with the measured coefficients in TrGO bulk films. The thermoelectric properties of the measured and calculated coefficients showed similar trends with increasing reduction temperature, and the charged carrier transport (i.e., the energy states) of TrGO can be tuned by varying the reduction temperature without doping with impurities.

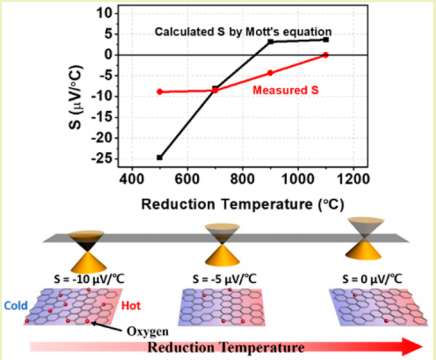

KEYWORDS: *Graphene oxide, Reduction degree, Seebeck coefficient, Field effect transistor, Mott's equation, Metallic conductor*

INTRODUCTION

The unique electrical properties of graphene have been studied since the discovery of this important material. Graphene is a two-dimensional material with sp^2 hybridization of its constituent carbon atoms. Although the outstanding and unique electrical properties of graphene are exploitable in flexible devices and transparent electrodes,[1,2] the applications of graphene sheets are limited in practice. For example, monolayer graphene sheets require a specialized fabrication method such as chemical vapor deposition (CVD), accompanied by a dedicated transfer process. These limitations can be overcome by graphene oxide (GO). The oxygen functional groups enable the dispersion of GO in water and hence the fabrication of large-area devices at low cost, and hydrogel, metal oxide or polymer composite.[3−8] To recover the sp^2 hybridization of graphene, the fabricated GO is subjected to a reduction process. Although the properties of reduced graphene oxide (rGO) and graphene are comparable, the electrical properties differ between the two materials. The unique physical properties of graphene are conferred by its fundamental properties such as zero bandgap and high mobility.[9−13] Unfortunately, the zero bandgap prohibits a proper on−off current ratio in graphene transistors. To open the bandgap in graphene, many researchers have applied structural engineering techniques.[14] In contrast, GO is synthesized by harsh oxidation from graphite, and the oxygen functional groups cause sp^3 bonding with subsequent surface defects. Oxidation increases the proportion of sp^3 bonds and disturbs the carrier transport. To control the reduction state of rGO, we must determine the electrical properties of rGO, which reflect the recovery of sp^2 hybridization.[15] Obtaining semiconducting rGO is a challenging task because the shape of graphene or the number of defects determines the density of states with bandgaps and zero bandgap.[16,17] These conclusions were theoretically inferred from reports (excluding reports on graphene nanoribbons[18,19]). As indicated above, the harsh conditions of GO synthesis induce random defects and oxygen functional groups. After reduction, the electrical properties of GO change from insulating to semimetal.[20] Although this transition can be

Received: January 8, 2018
Revised: March 14, 2018
Published: May 2, 2018

DOI: 10.1021/acssuschemeng.8b00094
ACS Sustainable Chem. Eng. 2018, 6, 7468−7474

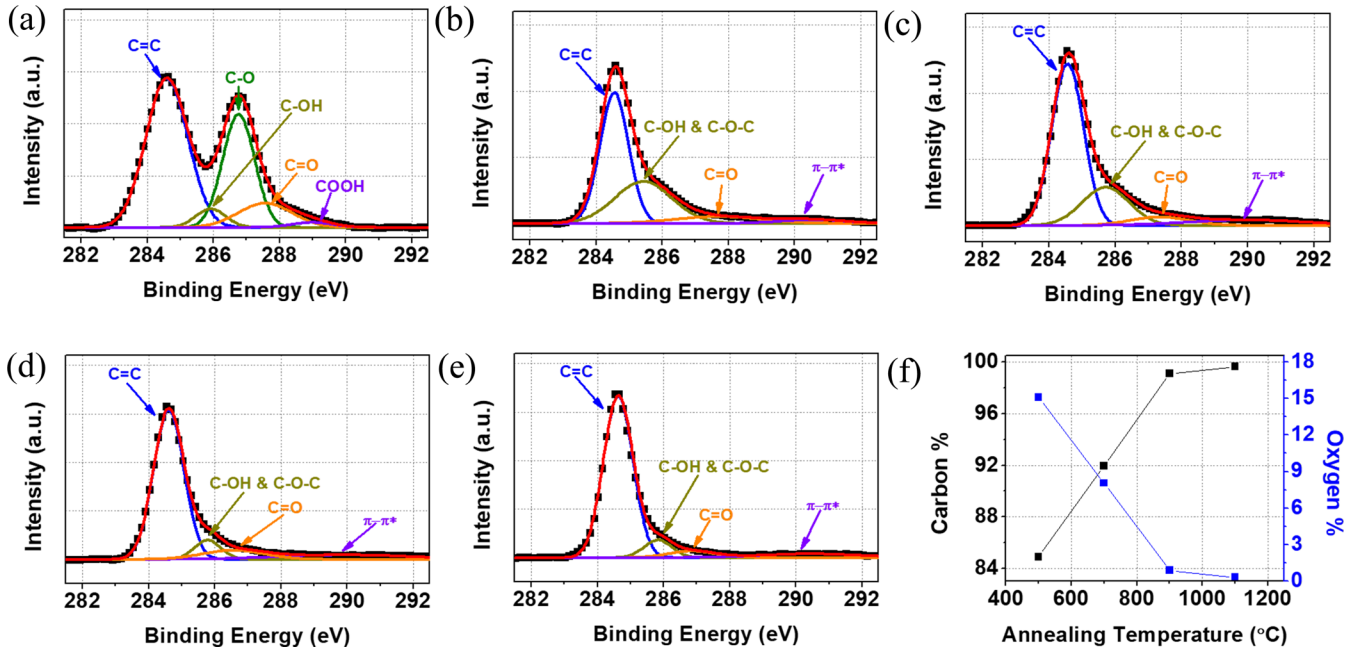

Figure 1. X-ray photoelectron spectroscopy spectra of (a) GO, (b) TrGO500, (c) TrGO700, (d) TrGO900, (e) TrGO1100, and (f) atomic ratio of carbon and oxygen from the elementary analysis.

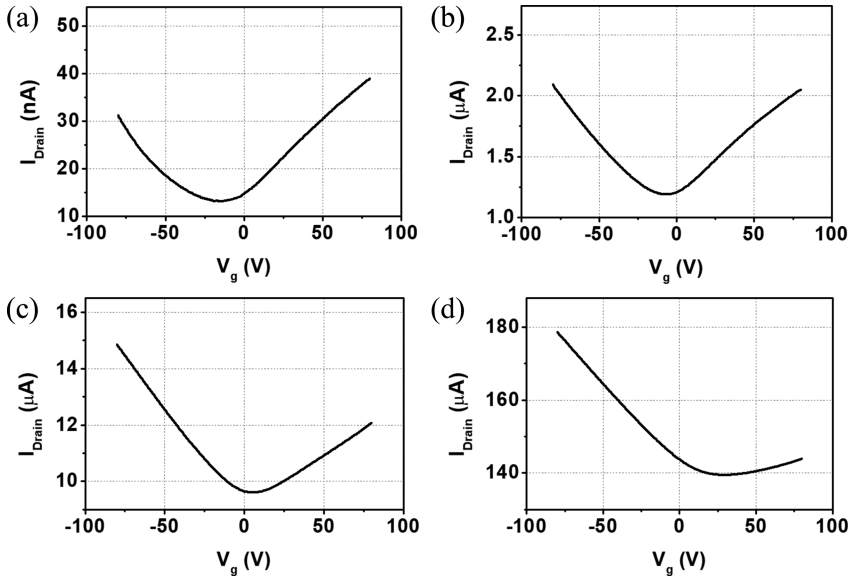

Figure 2. Transfer curves of (a) TrGO500, (b) TrGO700, (c) TrGO900, and (d) TrGO1100 with V_{Drain} = −1 V at room temperature.

controlled by altering the reduction degree, the residual-oxygen functional groups impede the electrical conduction of GO.

The Seebeck coefficient is useful for understanding the transport of charged carriers and the electronic structure of materials. The Seebeck coefficient of graphene depends on the sample preparation method. For example, the Seebeck coefficient of graphene exfoliated mechanically from graphite is nearly 0 μV/°C at zero bias voltage,[21] whereas that of graphene synthesized by CVD ranges from −40 to 50 μV/°C. These differences are caused by structural defects or different numbers of layers.[22,23] The Seebeck coefficient of rGO appears to be more complicated than that of graphene because the former possesses structural defects and residual-oxygen functional groups. Consequently, the structural shape and numbers of oxygen functional groups of rGO (which affect the Seebeck coefficient) are difficult to control. Choi et al. reported that the Seebeck coefficient of rGO was changed from 60 to 10 μV/°C as a function of reduction degree (i.e., the amount of hydrazine).[24] In rGO reduced by thermal annealing, the Seebeck coefficient was found to fluctuate with increasing reduction temperature.[25] Park et al. recently reported thermoelectric properties of rGO annealed at 1000 °C in Ar/H_2 atmosphere, as a function of ambient temperature.[26]

In the present study, the charge-carrier transport properties of thermally reduced rGO were monitored as functions of the reduction temperature. To this end, field effect transistors (FETs) were fabricated from thermally reduced GO (TrGO) at 500, 700, 900, and 1100 °C, respectively, and their transfer curves were measured as functions of gate bias (V_g). The carrier transport properties of the FETs were also investigated.

DOI: 10.1021/acssuschemeng.8b00094
ACS Sustainable Chem. Eng. 2018, 6, 7468−7474

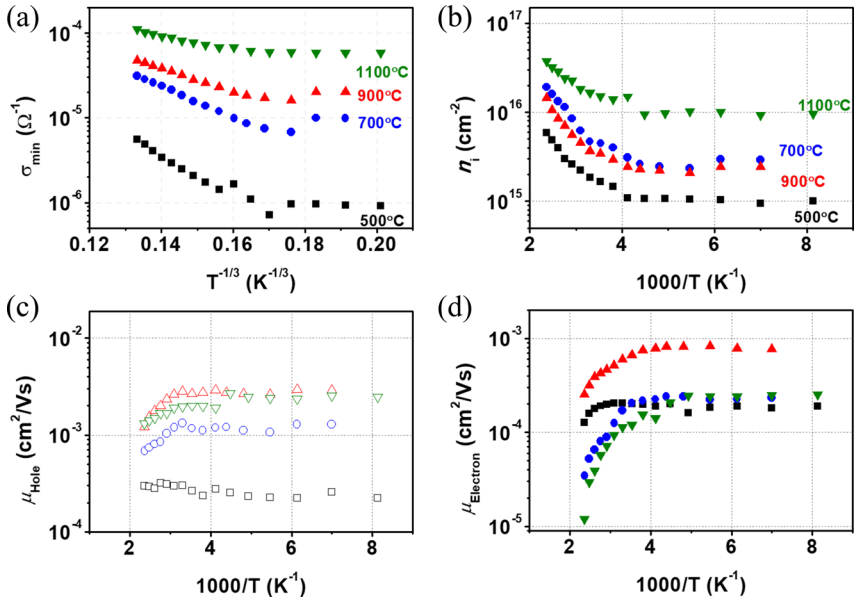

Figure 3. Temperature dependence of (a) minimum conductivity of TrGO versus $T^{-1/3}$, (b) Arrhenius plot of intrinsic carrier density, and field effect mobilities of (c) holes and (d) electrons versus $1000/T$.

Moreover, to evaluate the contributions of electron- or hole-transport in the TrGOs, we estimated the Seebeck coefficients from the transfer curves by Mott's equation at V_g = 0 V and compared them with the measured Seebeck coefficients in TrGO bulk films. From the transfer curves and Seebeck coefficients, the energy-level shifts of the charge neutrality point (E_{CNP}) and the Fermi-level (E_F) in the TrGOs were computed. The results confirmed that thermally reducing rGO at different temperatures is equivalent to modulating the doping level in TrGO.

RESULTS AND DISCUSSION

Figure 1 displays the XPS spectra of GO and the TrGOs thermally reduced at 500, 700, 900, and 1100 °C. In GO, the binding energies of C═C, C−OH, C−O, C═O, and COOH peaked at 284.5, 285.9, 286.7, 287.6, and 289 eV, respectively. The carbon- and oxygen-containing functional groups were clearly detected in GO, but their peaks were diminished after thermal reduction. The GO spectrum was dominated by C═C and C−O, whereas the TrGO500, TrGO700, TrGO900, and TrGO1100 spectra were dominated only by C═C bonding. Furthermore, the area under the C═C peak continuously increased with reduction temperature, indicating enhancement of the sp^2 hybridization of C═C. The C, H, O, and N contents of the materials were then examined by elementary analysis. As the reduction temperature increased, the carbon contents increased from 85% in TrGO500 to 99% in TrGO1100, whereas the oxygen contents reduced from approximately 15% in TrGO500 to 0.3% in TrGO1100. As the thermal reduction process was conducted in an Ar atmosphere, no nitrogen was detected in either the XPS spectra or the elementary analysis. In both analyses, the reduced oxygen contents at higher reduction temperatures confirmed the thermal reduction of GO.

To investigate how the charge-carrier transport properties of TrGO depend on reduction temperature, we obtained the transfer curves of TrGO500, TrGO700, TrGO900, and TrGO1100 at room temperature (Figure 2). In obtaining transfer curves, the TrGO transistor was prepared on patterned electrode by the spin-coating method. TrGO flakes were covered evenly on the substrate. (Figure S1) Although all TrGOs exhibited a typical ambipolar field effect, their on−off ratios were very small. The drain current level at the charge neutrality point (CNP) increased from 13 nA to 140 μA as the reduction temperature increased from 500 to 1100 °C. This indicates that our TrGOs have almost zero bandgap or metallic bandgap structures. The V_g at the CNP shifted from negative to positive between 700 and 900 °C, indicating that as the reduction temperature increased, the increased drain current was related to enhanced hole transport. This shifted E_{CNP} was suspected to be associated with the doping effect of the residual-oxygen functional groups or the structural defects on the TrGO surface during thermal reduction. As observed above, the oxygen contents in TrGO became lower as the reduction temperature increased, indicating greater removal of the oxygen-containing functional groups. The ambipolar behavior in the transfer curves indicates that reduced GO transports both electron and holes, and the hole current intensifies with increasing reduction temperature. To understand the effect of electron and hole transport on the thermoelectric performances of the TrGOs, the Seebeck coefficient of each TrGO was estimated from its transfer curve and compared with that measured in the corresponding TrGO bulk film. The Seebeck coefficient was chosen for this purpose because it reflects the species of charge carriers in materials. Depending on the electronic structure of the investigated material (insulating, semiconducting, or conducting), the Seebeck coefficient has been variously expressed as a function of Fermi-level (E_F), transport mechanism, band gap width, and others.[27−29] Therefore, before calculating the Seebeck coefficient of TrGO precisely from the transfer curve, we should clarify the electronic structure of TrGO.

To clarify the electronic structure of TrGO, we determined the minimum conductances (Ω_{min}^{-1}), intrinsic carrier densities (n_i), and mobilities of TrGO500, TrGO700, TrGO900, and TrGO1100 as functions of $T^{-1/3}$ or $1000/T$, where T is the ambient temperature.[20] Depending on the ambient temperature, transfer curves were obtained with all samples (Figure S2), and then carrier densities and mobilities were calculated.

DOI: 10.1021/acssuschemeng.8b00094
ACS Sustainable Chem. Eng. 2018, 6, 7468−7474

The results are plotted in Figure 3. As shown in the Arrhenius plots of Figure 3a, the electrical conductance Ω_{min}^{-1} was enhanced in TrGOs that were thermally reduced at higher temperature. Despite this trend, the curves of all samples exhibited two regions with different slopes. More precisely, the conductance remained relatively steady in the low-temperature region (<−65 °C) but increased steadily in the high-temperature region (> −65 °C). This indicates that the Arrhenius model well fits the minimum conductance at ambient temperatures above 65 °C. The near-zero activation energy in the low-temperature region indicates a monotonous density of states in the TrGOs. At elevated temperature, the conduction in TrGO was dominated by thermally excited carriers, suggesting a nonmonotonous density of states in the TrGOs. The crossover temperature decreases in highly reduced GOs, indicating a band-like transport due to the healing effect of the sp^2 network structure.[20]

Over the ambient temperature range, the intrinsic carrier density n_i was larger in TrGOs thermally reduced at higher temperatures. The exception was TrGO700, with a slightly higher n_i than TrGO900. In the low-temperature region, the n_i remained steady in all samples, indicating no activation energy in the carrier transports. Generally, the oxygen-containing functional groups on the surfaces of GOs express poor sp^2 hybridization, but when the reduction process is started, sp^2 hybridization is generated. Increasing the sp^2 hybridization induces metallic conduction in the TrGO.

The field effect mobilities of the electrons and holes were observed (Figure 3c,d). Over the ambient temperature range, the carrier mobilities of electron and hole were approximately 10^{-4}−10^{-2} and 10^{-5}−10^{-3} $cm^2/(V\ s)$, respectively, much lower than in single-layer graphene (reported as ~10^4 $cm^2/(V\ s)$).[30] In the present study, the mobilities are hindered by contact resistance among the stacked TrGO layers. The overall mobilies in all TrGOs significantly decreased as the ambient temperature increased[31] because of increased scattering at higher temperature. In TrGO films reduced at higher temperature, the decrease in hole and electron mobilities was enhanced. Especially, electron mobilities were dropped much more significantly than hole mobilities at $1000/T < 4$. It means that the electron transport was much more suppressed in TrGO films reduced at higher temperature due to the change in energy states.

The on−off ratios of the TrGOs in Figure 2 are very low; moreover, the TrGOs conducted at low temperature, where their electrons could not be thermally excited (see Figure 3a). Therefore, the Seebeck coefficient of TrGO can be determined by the following Mott's equation:

$$S = -\frac{\pi^2 k_B^2 T}{3e}\left[\frac{d\ln G(E)}{dE}\right]_{E=E_F} \quad (1)$$

where k_B and T are Boltzmann's constant and the absolute temperature, respectively, and e and E_F have been defined above.

For application to the present study, the Mott's equation was transformed as follows:

$$S = -\frac{\pi^2 k_B^2 T}{3e}\frac{1}{G}\frac{dG}{dV_g}\frac{dV_g}{dE}\bigg|_{E=E_F} \quad (2)$$

where G and V_g are the conductance and gate voltage of the transistor, respectively.[21]

Here, values for $(1/G)\cdot(dG/dV_g)\cdot(dV_g/dE)$ were obtained from the differential value in a plot of ln G vs E, i.e., the log scale plot of transfer curves at 25 °C. Then, Seebeck coefficients of the TrGOs were calculated using eq 2 and are plotted as functions of V_g in Figure 4. The dependence of the Seebeck

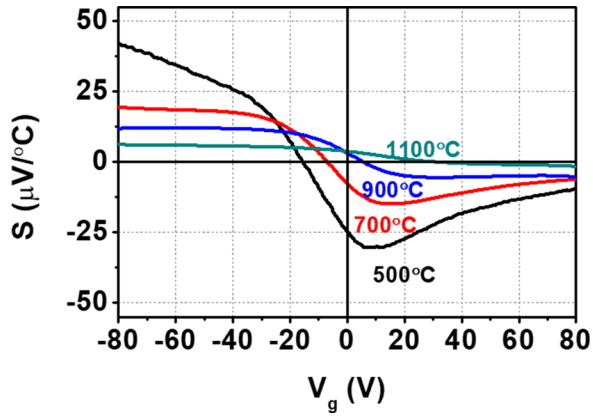

Figure 4. Seebeck coefficients calculated from the transfer curves at room temperature by a modified Mott eq (eq 2).

coefficient on V_g results from the changing Fermi-level (E_F) in the TrGOs. In general, the absolute value of the Seebeck coefficient decreased with increasing reduction temperature, and the Seebeck coefficients of all TrGO samples exhibited both n- and p-type characteristics, reflecting the ambipolar property in their transfer curves. In detail, the Seebeck coefficient of TrGO500 at 25 °C varied from 42 to −30 μV/°C across the range of V_g. The Seebeck coefficient changed sign, implying that the charged carriers in the TrGO500 changed from holes (positive carriers) to electrons (negative carriers), depending on the E_F in the sample. However, the Seebeck coefficients of the other samples showed different behaviors. As the reduction temperature increased, the Seebeck coefficients in both the hole- and electron-transport regimes approached 0 μV/°C, as suspected by the higher conductance in TrGO at higher reduction temperatures.

Figure 5 compares the Seebeck coefficients calculated from Mott's equation with those in bulk film measured at room temperature. The Seebeck coefficients of the samples were calculated at V_g = 0 V because the Seebeck coefficient of bulk film was measured without applying V_g. Seebeck coefficient of bulk film was obtained by plotting potential gradient as a function of temperature gradient as displayed in Figure S3 and these plots are shown in Figure S4. Although the calculated and measured Seebeck coefficients were mismatched, they showed similar tendencies. The differences can be attributed to different sample preparations and electric fields in the channel direction. In both cases, the Seebeck coefficient changed from negative to positive as the reduction temperature increased.

Next, we compared the Seebeck coefficients with the transfer curves. The transfer curve of TrGO500 showed ambipolar properties, indicating that both electrons and holes were transported. However, the Seebeck coefficients calculated by Mott's equation and measured in bulk film were both negative at V_g = 0 V, indicating that the major charged carriers were electrons.

According to several reports, the thermoelectric properties of carbon-based materials are determined by the doping state of the materials.[32,33] The transfer curve of carbon nanotubes

DOI: 10.1021/acssuschemeng.8b00094
ACS Sustainable Chem. Eng. 2018, 6, 7468−7474

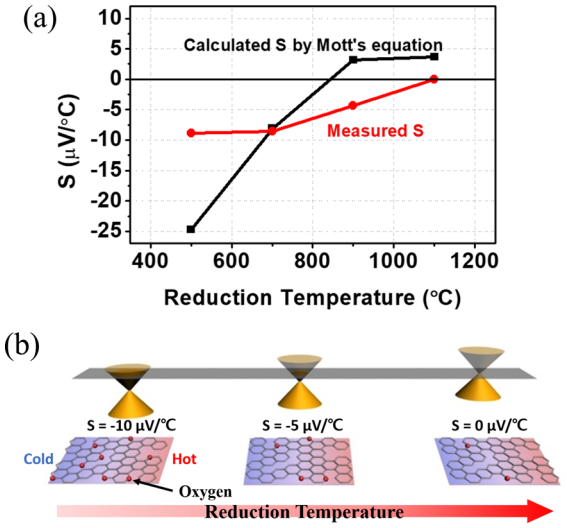

Figure 5. (a) Comparison of Seebeck coefficients calculated by Mott's equation and measured in bulk film at room temperature. (b) Schematic of changes in the energy band structure of rGO with increasing reduction temperature.

shows an ambipolar shape,[34−36] but in an ambient environment (without V_g), the carbon nanotubes are intrinsically in the hole-doped state; in other words, the Seebeck coefficient of intrinsic carbon nanotubes is positive.[37,38] The E_{CNP} of graphene or rGO is readily shifted by attaching nanoparticles or silane-based materials.[39,40] Moreover, the residual-oxygen functional groups reportedly alter the work function of rGO.[41,42] In general, the E_{CNP} and work function of graphene exfoliated from graphite appear at similar positions. However, when the rGO lattice is doped with impurities such as boron or nitrogen atoms, a gap appears between E_F and E_{CNP}, which is known as the doping state.[43]

The present study suggests that the difference between E_F (at V_g = 0 V) and the energy level of the CNP (E_{CNP}) plays an important role in determining the sign and absolute value of the Seebeck coefficient (see Figure 5b). As revealed in the transfer curves, the E_{CNP} was increased in TrGOs reduced at higher temperature. Moreover, high reduction temperatures produced a doping effect despite the lack of doping impurities. This effect is suspected to be caused by the removal of residual oxygen and the healing of structural defects on the TrGOs. The TrGOs reduced at all temperatures were metallically conducting. As the reduction temperature increased, the E_{CNP} and E_F converged toward a similar level, meaning that the structure approached that of ideal graphene (that is, a perfect sp^2 network structure). In conclusion, we found that controlling the positions of E_F and E_{CNP} in rGO was important for determining their Seebeck coefficients in the metallic conducting regime.

CONCLUSIONS

In summary, the charge-carrier transport properties of TrGO were investigated as functions of the reduction temperature. Most importantly, we found that the Seebeck coefficients of TrGO can be changed by controlling the reduction temperature, which induces a shift from E_{CNP} to E_F without doping with impurities or other elements. The transfer curves revealed both electron and hole transport in TrGO, although hole transport dominated at higher reduction temperatures. Furthermore, after we examined the Arrhenius plots of carrier density and carrier mobility, we determined that TrGO behaved as a metallic conductor at all investigated reduction temperatures. As the Seebeck coefficient calculated by Mott's equation assumes a material with metallic conduction, it was calculated from the electric conductance of TrGO. According to the modified Mott's equation, the Seebeck coefficient changed sign at the CNP, and its magnitude depended on the energy level (V_g). For comparison, the actual Seebeck coefficient was measured in TrGO bulk films. Both the Seebeck coefficients calculated by Mott's equation at E_F (V_g = 0 V) and the measured Seebeck coefficients in bulk films exhibited similar behaviors, namely, their absolute values decreased and reached zero at a sufficiently high reduction temperature. This means that E_{CNP} and E_F converge to a common level as the reduction temperature increases, and the TrGO structure develops an ideal graphene structure (i.e., a perfect sp^2 network structure). In conclusion, we found that controlling the positions of E_F and CNP in rGO is important for determining the Seebeck coefficient in metallically conducting rGO.

EXPERIMENTAL SECTION

Fabrication of Graphite Oxide and Graphene Oxide Solution. GO was prepared from graphite powder by Hummer's method. Briefly, 1 g of graphite powder (SP-1, Bay Carbon Inc., U.S.A.) and 0.5 g of $NaNO_3$ were dissolved in H_2SO_4 (25 mL) with stirring for 1 h, maintaining the reaction flask in an ice bath. Next, 3 g of $KMnO_4$ was added to the mixture with stirring for another hour, while the temperature was gradually increased to 35 °C. After consecutively adding H_2O (46 mL) and mixed H_2O and H_2O_2 (140 and 2.5 mL, respectively), the mixture was washed with 10% HCl solution and D.I. water. Finally, the wet product was freeze-dried for obtaining GO powders. After drying, 20 mg of the GO powder was dispersed in 20 mL of H_2O by bath-sonication, followed by centrifuging at 3000 rpm for 5 min. The supernatant was collected in a vial. The morphology of GO flakes was observed by atomic force microscopy (AFM) and 1 nm thickness and ∼1 μm size of GO was obtained. (Figure S5)

Fabrication of FET. To investigate the charge-carrier transport properties of TrGO, FETs were prepared. The GO solution was spin-coated at 1000 rpm (30 s) and 2000 rpm (20 s) onto cleaned Si/SiO_2 substrates (thickness of 300 nm). This process was conducted five times. Next, the GO on the substrates was reduced at 500, 700, 900, or 1100 °C for 2 h in an Ar atmosphere. After reduction, separated channels were patterned in the thermally reduced GO film by photolithography. The residual parts were etched by O_2 plasma. The electrodes (Au; thickness 50 nm) of the FETs were deposited by thermal evaporation.

Fabrication of TrGO Bulk Film. A TrGO bulk film was prepared by the vacuum filtration method. The GO solution was prepared as mentioned above. The GO film was obtained on poly tetrafluoroethylene (PTFE) membrane (0.2 μm; Omnipore). The film was dried in a vacuum oven for 24 h at 80 °C. After removing the membrane, the bulk GO film was reduced at 500, 700, 900, or 1100 °C for 2 h in an Ar atmosphere.

Characterization. Reduction of GO was confirmed by X-ray photoelectron spectroscopy (XPS, PHI 5000, Ulvac PHI, Japan). The percentages of carbon, hydrogen, nitrogen, and sulfur were measured by a CHNS analyzer (FLASH 2000; Thermo Scientific, U.K.), and the oxygen percentage was determined by an O analyzer (EA 1108; Fison Instruments, Italy). AFM (SPA-400, Seiko instrument) was used for morphology of TrGO. The electrical performances of the FETs were measured by a semiconductor parameter analyzer (Keithly 4200C) under high-vacuum conditions (∼10^{-6} Torr). Transfer curve of TrGO was obtained with applying −1 V of drain bias (V_d), and the sweep of gate vias (V_g) was applied from 80 to −80 V. When obtaining the Arrhenius plots, the ambient temperature was controlled with liquid

DOI: 10.1021/acssuschemeng.8b00094
ACS Sustainable Chem. Eng. 2018, 6, 7468−7474

nitrogen. The field effect mobility (μ) and intrinsic carrier concentration (n_i) were, respectively, calculated as

$$\mu = \frac{dI_d}{dV_g}\frac{L}{W}\frac{1}{C_{ox}V_d} \quad (3)$$

$$n_i = \frac{\sigma_{min}}{e(\mu_{hole} + \mu_{electron})} \quad (4)$$

where I_{Drain}, V_{Gate}, C_{ox}, and V_{Drain} are the drain current, gate voltage, gate oxide capacitance, and drain voltage, respectively. L and W are the length and width of the channel, respectively, and σ_{min} and e denote the minimum conductance and unit electrical charge, respectively.[31]

The Seebeck coefficient of the bulk TrGO film was determined by plotting the thermal voltage versus temperature under low-vacuum conditions (~10^{-3} Torr). The temperature gradient was applied by a ceramic heating block. The temperature was detected by a type-R thermocouple (+: Pt/Rh = 87/13 w/w, -: Pt) connected to a data acquisition/data logger switch unit (Agilent 34970A, Agilent Technologies, Inc., United States). The slope of the potential plotted against the difference (ΔT) from the specified temperature (±3 °C) yielded the Seebeck coefficient.

■ ASSOCIATED CONTENT

Supporting Information

The Supporting Information is available free of charge on the ACS Publications website at DOI: 10.1021/acssuschemeng.8b00094.

Additional figures and experimental details (PDF)

■ AUTHOR INFORMATION

Corresponding Author

*E-mail: hyunjung@kookmin.ac.kr.

ORCID

Hyunwoo Bark: 0000-0002-4203-751X
Mijung Lee: 0000-0002-9677-5788
Wonmok Lee: 0000-0001-6757-885X
Byunghee Hong: 0000-0001-8355-8875

Notes

The authors declare no competing financial interest.

■ ACKNOWLEDGMENTS

We thank to Dr. Deepak Venkateshvaran for helpful discussion. This research was supported by Basic Science Research Program through the National Research Foundation of Korea (NRF) funded by the Ministry of Science and ICT (NRF-2017R1A2B2010552 and 2015R1A5A7037615) and Civil Military Technology Cooperation Center (15-CM-SS-03 and 15-CM-EN-08).

■ REFERENCES

(1) Li, X.; Zhu, Y.; Cai, W.; Borysiak, M.; Han, B.; Chen, D.; Piner, R. D.; Colombo, L.; Ruoff, R. S. Transfer of Large-Area Graphene Films for High-Performance Transparent Conductive Electrodes. *Nano Lett.* **2009**, *9* (12), 4359.

(2) Pang, S.; Hernandez, Y.; Feng, X.; Müllen, K. Graphene as Transparent Electrode Material for Organic Electronics. *Adv. Mater.* **2011**, *23* (25), 2779.

(3) Eda, G.; Chhowalla, M. Chemically Derived Graphene Oxide: Towards Large-Area Thin-Film Electronics and Optoelectronics. *Adv. Mater.* **2010**, *22* (22), 2392.

(4) Wang, S.; Ang, P. K.; Wang, Z.; Tang, A. L. L.; Thong, J. T. L.; Loh, K. P. High Mobility, Printable, and Solution-Processed Graphene Electronics. *Nano Lett.* **2010**, *10* (1), 92.

(5) Sung, Y.; Kim, T.-H.; Lee, B. Syntheses of carboxymethylcellulose/graphene nanocomposite superabsorbent hydrogels with improved gel properties using electron beam radiation. *Macromol. Res.* **2016**, *24* (2), 143.

(6) Choi, S.-M.; Park, S.-Y. Ultraviolet-assisted reduction of BBL/graphene nanocomposite. *Macromol. Res.* **2015**, *23* (5), 428.

(7) Fan, Y.; Kang, L.; Zhou, W.; Jiang, W.; Wang, L.; Kawasaki, A. Control of doping by matrix in few-layer graphene/metal oxide composites with highly enhanced electrical conductivity. *Carbon* **2015**, *81*, 83.

(8) Wang, W.; Zhang, Q.; Li, J.; Liu, X.; Wang, L.; Zhu, J.; Luo, W.; Jiang, W. An efficient thermoelectric material: preparation of reduced graphene oxide/polyaniline hybrid composites by cryogenic grinding. *RSC Adv.* **2015**, *5* (12), 8988.

(9) Das Sarma, S.; Adam, S.; Hwang, E. H.; Rossi, E. Electronic transport in two-dimensional graphene. *Rev. Mod. Phys.* **2011**, *83* (2), 407.

(10) Kim, S.; Nah, J.; Jo, I.; Shahrjerdi, D.; Colombo, L.; Yao, Z.; Tutuc, E.; Banerjee, S. K. Realization of a high mobility dual-gated graphene field-effect transistor with Al_2O_3 dielectric. *Appl. Phys. Lett.* **2009**, *94* (6), 062107.

(11) Meric, I.; Han, M. Y.; Young, A. F.; Ozyilmaz, B.; Kim, P.; Shepard, K. L. Current saturation in zero-bandgap, top-gated graphene field-effect transistors. *Nat. Nanotechnol.* **2008**, *3* (11), 654.

(12) Shin, K.-Y.; Lee, S. Y.; Lee, S.-S. Implication of mesoporous 3-D graphene skeleton platform based on interconnected framework architecture in constructing electro-conductive flexible nanocomposites. *Macromol. Res.* **2016**, *24* (2), 170.

(13) Lee, E. G.; Shin, K.-Y.; Lee, J.; Lee, S.-S. Flexible free-standing composite films having 3D continuous structures of hollow graphene ellipsoids. *Macromol. Res.* **2015**, *23* (6), 552.

(14) Li, X.; Wang, X.; Zhang, L.; Lee, S.; Dai, H. Chemically Derived, Ultrasmooth Graphene Nanoribbon Semiconductors. *Science* **2008**, *319* (5867), 1229.

(15) Mattevi, C.; Eda, G.; Agnoli, S.; Miller, S.; Mkhoyan, K. A.; Celik, O.; Mastrogiovanni, D.; Granozzi, G.; Garfunkel, E.; Chhowalla, M. Evolution of Electrical, Chemical, and Structural Properties of Transparent and Conducting Chemically Derived Graphene Thin Films. *Adv. Funct. Mater.* **2009**, *19* (16), 2577.

(16) Wang, S.; Chia, P.-J.; Chua, L.-L.; Zhao, L.-H.; Png, R.-Q.; Sivaramakrishnan, S.; Zhou, M.; Goh, R. G. S.; Friend, R. H.; Wee, A. T. S.; Ho, P. K. H. Band-like Transport in Surface-Functionalized Highly Solution-Processable Graphene Nanosheets. *Adv. Mater.* **2008**, *20* (18), 3440.

(17) Guo, L.; Shao, R.-Q.; Zhang, Y.-L.; Jiang, H.-B.; Li, X.-B.; Xie, S.-Y.; Xu, B.-B.; Chen, Q.-D.; Song, J.-F.; Sun, H.-B. Bandgap Tailoring and Synchronous Microdevices Patterning of Graphene Oxides. *J. Phys. Chem. C* **2012**, *116* (5), 3594.

(18) Liang, X.; Jung, Y.-S.; Wu, S.; Ismach, A.; Olynick, D. L.; Cabrini, S.; Bokor, J. Formation of Bandgap and Subbands in Graphene Nanomeshes with Sub-10 nm Ribbon Width Fabricated via Nanoimprint Lithography. *Nano Lett.* **2010**, *10* (7), 2454.

(19) Ouyang, Y.; Yoon, Y.; Guo, J. Scaling Behaviors of Graphene Nanoribbon FETs: A Three-Dimensional Quantum Simulation Study. *IEEE Trans. Electron Devices* **2007**, *54* (9), 2223–2231.

(20) Eda, G.; Mattevi, C.; Yamaguchi, H.; Kim, H.; Chhowalla, M. Insulator to Semimetal Transition in Graphene Oxide. *J. Phys. Chem. C* **2009**, *113* (35), 15768.

(21) Zuev, Y. M.; Chang, W.; Kim, P. Thermoelectric and Magnetothermoelectric Transport Measurements of Graphene. *Phys. Rev. Lett.* **2009**, *102* (9), 096807.

(22) Cho, S.; Kang, S. D.; Kim, W.; Lee, E.-S.; Woo, S.-J.; Kong, K.-J.; Kim, I.; Kim, H.-D.; Zhang, T.; Stroscio, J. A.; Kim, Y.-H.; Lyeo, H.-K. Thermoelectric imaging of structural disorder in epitaxial graphene. *Nat. Mater.* **2013**, *12* (10), 913.

(23) Xiao, N.; Dong, X.; Song, L.; Liu, D.; Tay, Y.; Wu, S.; Li, L.-J.; Zhao, Y.; Yu, T.; Zhang, H.; Huang, W.; Hng, H. H.; Ajayan, P. M.; Yan, Q. Enhanced Thermopower of Graphene Films with Oxygen Plasma Treatment. *ACS Nano* **2011**, *5* (4), 2749.

DOI: 10.1021/acssuschemeng.8b00094
ACS Sustainable Chem. Eng. 2018, 6, 7468–7474

(24) Choi, J.; Tu, N. K.; Lee, S.-S.; Lee, H.; Kim, J.; Kim, H. Controlled oxidation level of reduced graphene oxides and its effect on thermoelectric properties. *Macromol. Res.* **2014**, *22* (10), 1104.
(25) Tu, N. D. K.; Choi, J.; Park, C. R.; Kim, H. Remarkable Conversion Between n- and p-Type Reduced Graphene Oxide on Varying the Thermal Annealing Temperature. *Chem. Mater.* **2015**, *27* (21), 7362.
(26) Park, M.; Hong, S. J.; Kim, K. H.; Kang, H.; Lee, M.; Jeong, D. H.; Park, Y. W.; Kim, B. H. Electrical and thermoelectric transport by variable range hopping in reduced graphene oxide. *Appl. Phys. Lett.* **2017**, *111* (17), 173103.
(27) Cutler, M.; Mott, N. F. Observation of Anderson Localization in an Electron Gas. *Phys. Rev.* **1969**, *181* (3), 1336.
(28) Pernstich, K. P.; Rossner, B.; Batlogg, B. Field-effect-modulated Seebeck coefficient in organic semiconductors. *Nat. Mater.* **2008**, *7* (4), 321.
(29) Venkateshvaran, D.; Nikolka, M.; Sadhanala, A.; Lemaur, V.; Zelazny, M.; Kepa, M.; Hurhangee, M.; Kronemeijer, A. J.; Pecunia, V.; Nasrallah, I.; Romanov, I.; Broch, K.; McCulloch, I.; Emin, D.; Olivier, Y.; Cornil, J.; Beljonne, D.; Sirringhaus, H. Approaching disorder-free transport in high-mobility conjugated polymers. *Nature* **2014**, *515* (7527), 384.
(30) Novoselov, K. S.; Geim, A. K.; Morozov, S. V.; Jiang, D.; Zhang, Y.; Dubonos, S. V.; Grigorieva, I. V.; Firsov, A. A. Electric Field Effect in Atomically Thin Carbon Films. *Science* **2004**, *306* (5696), 666.
(31) Kobayashi, T.; Kimura, N.; Chi, J.; Hirata, S.; Hobara, D. Channel-Length-Dependent Field-Effect Mobility and Carrier Concentration of Reduced Graphene Oxide Thin-Film Transistors. *Small* **2010**, *6* (11), 1210.
(32) Xu, K.; Zeng, C.; Zhang, Q.; Yan, R.; Ye, P.; Wang, K.; Seabaugh, A. C.; Xing, H. G.; Suehle, J. S.; Richter, C. A.; Gundlach, D. J.; Nguyen, N. V. Direct Measurement of Dirac Point Energy at the Graphene/Oxide Interface. *Nano Lett.* **2013**, *13* (1), 131.
(33) Yin, L.-C.; Cheng, H.-M.; Saito, R.; Dresselhaus, M. S. Fermi level dependent optical transition energy in metallic single-walled carbon nanotubes. *Carbon* **2011**, *49* (14), 4774.
(34) Derenskyi, V.; Gomulya, W.; Rios, J. M. S.; Fritsch, M.; Fröhlich, N.; Jung, S.; Allard, S.; Bisri, S. Z.; Gordiichuk, P.; Herrmann, A.; Scherf, U.; Loi, M. A. Carbon Nanotube Network Ambipolar Field-Effect Transistors with 10^8 On/Off Ratio. *Adv. Mater.* **2014**, *26* (34), 5969.
(35) Lee, S.-H.; Khim, D.; Xu, Y.; Kim, J.; Park, W.-T.; Kim, D.-Y.; Noh, Y.-Y. Simultaneous Improvement of Hole and Electron Injection in Organic Field-effect Transistors by Conjugated Polymer-wrapped Carbon Nanotube Interlayers. *Sci. Rep.* **2015**, *5*, ArticleNo. 10407 DOI: 10.1038/srep10407.
(36) Yanagi, K.; Kanda, S.; Oshima, Y.; Kitamura, Y.; Kawai, H.; Yamamoto, T.; Takenobu, T.; Nakai, Y.; Maniwa, Y. Tuning of the Thermoelectric Properties of One-Dimensional Material Networks by Electric Double Layer Techniques Using Ionic Liquids. *Nano Lett.* **2014**, *14* (11), 6437.
(37) Hone, J.; Ellwood, I.; Muno, M.; Mizel, A.; Cohen, M. L.; Zettl, A.; Rinzler, A. G.; Smalley, R. E. Thermoelectric Power of Single-Walled Carbon Nanotubes. *Phys. Rev. Lett.* **1998**, *80* (5), 1042.
(38) Yu, C.; Shi, L.; Yao, Z.; Li, D.; Majumdar, A. Thermal Conductance and Thermopower of an Individual Single-Wall Carbon Nanotube. *Nano Lett.* **2005**, *5* (9), 1842.
(39) Kang, B.; Lim, S.; Lee, W. H.; Jo, S. B.; Cho, K. Work-Function-Tuned Reduced Graphene Oxide via Direct Surface Functionalization as Source/Drain Electrodes in Bottom-Contact Organic Transistors. *Adv. Mater.* **2013**, *25* (41), 5856.
(40) Wang, D.; Liu, X.; He, L.; Yin, Y.; Wu, D.; Shi, J. Manipulating Graphene Mobility and Charge Neutral Point with Ligand-Bound Nanoparticles as Charge Reservoir. *Nano Lett.* **2010**, *10* (12), 4989.
(41) Kumar, P. V.; Bernardi, M.; Grossman, J. C. The Impact of Functionalization on the Stability, Work Function, and Photoluminescence of Reduced Graphene Oxide. *ACS Nano* **2013**, *7* (2), 1638.
(42) Sygellou, L.; Paterakis, G.; Galiotis, C.; Tasis, D. Work Function Tuning of Reduced Graphene Oxide Thin Films. *J. Phys. Chem. C* **2016**, *120* (1), 281.
(43) Khan, F.; Baek, S.-H.; Kim, J. H. One-step and controllable bipolar doping of reduced graphene oxide using TMAH as reducing agent and doping source for field effect transistors. *Carbon* **2016**, *100*, 608.

DOI: 10.1021/acssuschemeng.8b00094
ACS Sustainable Chem. Eng. 2018, 6, 7468−7474